

THE ACQUISITION AND STATISTICAL ANALYSIS OF RAPID 3D FMRI DATA

Martin A. Lindquist¹, Cun-Hui Zhang², Gary Glover³ and Lawrence Shepp²

¹*Columbia University*, ²*Rutgers University* and ³*Stanford University*

Abstract: In this work, we introduce a new approach toward the acquisition and statistical analysis of fMRI data. Our acquisition strategy is based on repeatedly measuring the low spatial frequencies present in the MR signal, allowing us to obtain a low spatial resolution snapshot of the brain with extremely high temporal resolution (100 *ms* compared to the standard 2,000 *ms*). The increased resolution allows us to study changes in oxygenation in the 3D brain *immediately* following activation. This in turn opens the possibility of shifting the statistical analysis of brain function closer toward the actual time frame of the underlying neuronal activation driving the process than is possible in standard fMRI experiments. However, this ability necessitates the introduction of new statistical techniques for analyzing the resulting data. We introduce one such approach in this paper. The feasibility and efficiency of the combined acquisition and analysis technique is confirmed using data from a visual-motor and an auditory-motor-visual task. The results of these experiments provide a proof of concept of our combined rapid imaging and analysis technique. It also indicates that our approach may provide important information regarding the initial negative BOLD signal, which can be used to obtain *accurate* temporal ordering of the various regions of the brain involved in a cognition experiment. Conversely, we show that the conventional approach of studying the positive BOLD signal will, at times, give *inaccurate* temporal ordering of the same regions. Thus, we believe that our approach will become an important tool for studying any cognition task which involves rapid mental processing in more than one region.

Key words and phrases: Echo-volumar imaging, fMRI, negative dip, latency, rapid imaging, temporal resolution, time series analysis.

1. Introduction

Functional Magnetic Resonance Imaging (fMRI) is a noninvasive imaging technique that can be used to study mental activity in a person's brain. It builds on repeatedly imaging a 3D brain volume and studying localized changes in oxygenation. The technique has the potential to answer many important questions regarding the way the brain functions. The drawback to fMRI studies, as currently performed, is that its temporal resolution is too low to effectively answer many interesting questions regarding activation in the brain. In particular, with low time-resolution data, one faces the statistically intractable task of sorting

out possibly unknown confounding factors influencing the ordering of the time of brain activity across different regions of the brain. In this work we present a new acquisition and analysis technique for performing rapid 3D fMRI studies which could potentially alleviate many of these concerns.

fMRI is most commonly performed using blood oxygenation level-dependent (BOLD) contrast (Ogawa, Tank, Menon, Ellerman, Kim, Merkle and Ugurbil (1992), Ogawa, Lee and Barrere (1993) and Ogawa, Menon, Tank, Kim, Merkle, Ellerman, and Ugurbil (1993)) to study local changes in deoxyhemoglobin concentration in the brain. Neural activity leads to an increase in both the cerebral metabolic rate for oxygen ($CMRO_2$) and the supply of oxygen via the cerebral blood flow (CBF). The positive BOLD signal is believed to be the result of a transient uncoupling between $CMRO_2$ and the supply increase, causing a reduction in paramagnetic deoxyhemoglobin in the capillaries and venules, though it is important to note that alternative theories regarding this mechanism exist (e.g., Buxton and Frank (1997)). Most fMRI methods use the positive BOLD response to study the underlying neural activity. However, BOLD imaging based on the positive response is limited by the sluggish nature of the underlying evoked hemodynamic response to a neural event (or the hemodynamic response function, HRF), which peaks 5-8 seconds after that neural activity has peaked. Most statistical techniques for analyzing fMRI data are based on detecting this peak (e.g., Worsley and Friston (1995), Friston, Penny, Phillips, Kiebel, Hinton and Ashburner (2002); and Henson, Price, Rugg, Turner and Friston (2002)). Therefore, inference regarding where and when activation is taking place is based on oxygenation patterns mostly outside of the immediate vicinity of the underlying event on which we wish to base our conclusions (i.e., the neural activity).

Several studies have shown that $CMRO_2$ increases more rapidly than CBF in the time immediately following neural activity, giving rise to a decrease in the BOLD signal in the first 1-2 seconds following activation, called the initial negative BOLD response or the *negative dip* (Cho, Ro and Lim (1992), Ernst and Hennig (1994), Menon, Ogawa, Hu, Strupp, Andersen and Ugurbil (1995) Malonek and Grinvald (1996) and Yacoub, Le and Hu (1998)). The ratio of the amplitude of the dip compared to the positive BOLD signal depends on the strength of the magnet and has been reported to be roughly 20% at 3 Tesla (Yacoub, Le and Hu (1998)). There is also evidence that the dip is more localized to areas of neural activity (Yacoub, Le and Hu (1998), Duong, Kim, Ugurbil and Kim (2000), Kim, Duong and Kim (2000) and Thompson, Peterson and Freeman (2004)) than the subsequent rise which appears less spatially specific. Due in part to these reasons, the negative response has so far not been reliably observed and its existence remains controversial (Logothetis (2000)). However, if one could reliably measure these signals they would be better to use for tracking rapid neural

events than the positive BOLD response. Since the time to the peak positive BOLD response (time-to-peak) occurs in a larger time scale than the speed of brain operations, there is a great risk of unknown confounding factors influencing the ordering of time-to-peak in comparison to the ordering of the timing of brain activities in different regions of interest (ROIs). This is much less of a problem when studying the initial negative BOLD signal, as the negative dip occurs in a time scale closer to the neural activity. Hence, the development of rapid imaging techniques that are sensitive to the initial negative BOLD signal would be beneficial in obtaining accurate measures of the order of activity in various brain regions.

In fMRI, each 3D brain volume consists of one reconstruction of a magnetic resonance image (MRI). The reconstructed image consists of a number of uniformly spaced volume elements, or voxels, whose intensity represents the spatial distribution of the nuclear spin density within that particular voxel. The actual signal measurements (the raw data) are acquired by the MR scanner in the frequency-domain (k-space), which is typically sampled on a rectangular Cartesian grid, and then Fourier transformed into the spatial-domain (image-space). To make a single MR image, one needs to make a large number of individual k-space measurements. For example to fully reconstruct a 64×64 image, a total of 4,096 separate measurements are needed. A single 2D slice of this size takes about 100 *ms* to sample. The standard approach toward three-dimensional sampling is the acquisition of a stack of 2D slices (typically 20 or more), one after the other. Using this methodology, it usually takes up to 2 seconds to obtain a full scan of the brain, which does not provide sufficient temporal resolution to study the initial dip. As an alternative to multi-slice sampling, a more effective approach would be to directly sample in 3D k-space. There have been numerous attempts at sampling 3D k-space (e.g., Irarrazabal and Nishimura (1995), Sabat, Mir, Guarini, Guesalaga and Irarrazaval (2003) and Mir, Guesalaga, Spiniak, Guarini and Irarrazaval (2004)), but most have not been concerned with speeding up the sampling rate and ultimately have had similar constraints on the temporal resolution as the standard multi-slice approach. To ensure the maximal amount of speed-up, we suggest a technique that samples as large a portion of 3D k-space, as possible, in the time window typically allocated for sampling a single 2D slice. This approach necessitates the sacrifice of spatial resolution, as the number of sampled k-space points would be lower than that of standard sampling techniques, but would enable the acquisition of 3D data at an extremely high temporal resolution. This would allow us to obtain a snapshot of the 3D brain in a time frame that has previously not been possible.

The trade-off between spatial and temporal resolution is often used to increase the data sampling speed required in many applications. Since hardware

limitations set an ultimate physical limit for the imaging acquisition rate, k-space sampling must be economized to meet the demands for image resolution, signal-to-noise ratio, and acquisition speed for a specific experiment. In techniques such as the keyhole (van Vaals, Brummer, Dixon, Tuithof, Engels, Nelson, Gerety, Chezmar, and den Boer (1993) and Gao, Xiong, Lai, Haacke, Woldorff, Li and Fox (1996)), singular value decomposition (Zientara, Panych and Jolesz (1994) and Panych, Oesterle, Zientara and Hennig (1996)) and generalized series reconstruction (Liang and Lauterbur (1994)) methods, *a priori* information consisting of a high-resolution reference image is incorporated with the reduced sample k-space data in order to maintain the spatial resolution of the dynamic images. Multiple coil techniques such as SMASH (Sodickson and Manning (1997)) and SENSE (Pruessmann, Weiger, Scheidegger and Boesiger (1999)), can also be used to achieve reduction of k-space sampling. With multi-coil techniques, prior knowledge about RF field distributions or the image sensitivity of the coils is utilized for constructing images from under-sampled k-space data.

It should be noted that rapid imaging has additional benefits beyond those discussed above. For example, it allows for the efficient removal of physiological noise due to cardiac and respiratory effects. Since respiration gives rise to a periodic function, with a period length of approximately 3 seconds, the Nyquist criteria does not allow us to fully reconstruct the signal in a standard low resolution fMRI experiment. Rapid fMRI circumvents this issue and allows for efficient reconstruction of the underlying signal without aliasing. This is beneficial as it allows us to significantly clean up the fMRI signal prior to analysis and obtain more accurate estimates of the hemodynamic response function. In addition, rapid imaging alleviates issues related to the fact that spatially separate regions of the brain are sampled at different times, thus negating the need for slice-time correction. It may also allow for more accurate correction of subject motion, as movement occurring during the acquisition of each individual volume will be reduced.

In this work we suggest a novel approach toward acquiring, reconstructing and analyzing three-dimensional fMRI data which is sensitive to the initial negative BOLD response. It involves trading off spatial for temporal resolution, and focusing the statistical analysis on studying the initial negative BOLD signal. Using a new acquisition strategy, a small central region of 3D k-space can be sampled every 100 *ms*. We provide explicit and simple rules for designing three-dimensional k-space trajectories, as well as a straightforward reconstruction algorithm. Further, we provide a step-by-step guideline toward the statistical analysis of the resulting data. The acquisition of high frequency fMRI time series necessitates the development of new statistical tools for detecting when and

where activation is taking place, as most of our inference is based on studying the timing and amplitude of the initial negative dip across various brain regions. The feasibility of the approach is confirmed using data from a visual-motor task and an auditory-visual-motor task. While the existence of a negative dip in fMRI is still considered somewhat controversial, the data presented in this paper gives strong evidence for its existence in both sets of experiments. Although our experiments were performed on a single subject, they are done on different days and our statistical analyses confirm the negative dip based on all individual data sets. Further the results suggest that the initial negative BOLD response contains important information regarding the timing of activation, information that is confounded when studying the positive BOLD response.

2. Theory

In this section we provide a full theoretical blueprint for our approach toward the acquisition and statistical analysis of rapid 3D fMRI imaging data. We begin by introducing a new approach toward data acquisition which allows one to sample the central portion of 3D k-space with a temporal resolution of 100 *ms*. Thereafter, we discuss an efficient algorithm for reconstructing the resulting k-space data. Finally, we deal with issues that arise in the statistical analysis of the resulting high-frequency time series data. These issues include the effective removal of seasonal components due to heart-rate and respiration, as well as defining new metrics for comparing the timing of activation across various brain regions.

2.1. A 3D K-space sampling trajectory

Our approach toward k-space sampling attempts to sample as large a portion of 3D k-space as possible in the allocated time window. In order to effectively sample the data, new ways of transversing 3D k-space must be developed. In this section we discuss the constraints that any k-space trajectory must follow, and suggest a sampling trajectory for which these constraints hold. Using this trajectory allows us to obtain a snapshot of the 3D brain in a time frame that has previously not been possible, albeit at a lower spatial resolution than is standard in fMRI.

The 3D MRI Sampling Problem

In current implementations three-dimensional k-space sampling is typically performed by acquiring a stack of 2D slices, one after the other. Prior to acquisition of each slice, the nuclei are re-excited to ensure that a sufficiently strong

signal is available. Using this approach, it typically takes approximately 2 seconds to obtain a full scan of the brain and the resulting temporal resolution of the experiment is low. In addition the slices are sampled at different time points, which necessitates slice-time correction to ensure that the data accurately reflects the standard assumption that all voxels in the 3D brain were sampled instantaneously. As an alternative to the multi-slice approach, it would be more effective to directly sample a 3D region of k-space. In this paper we derive trajectories that can be used for single-shot (i.e., one re-excitation) imaging. This enables 3D fMRI studies to be performed at a high temporal resolution (e.g., 100 *ms* compared to 2,000 *ms*).

Our goal is to find a trajectory, $k(t)$, that moves through the central portion of 3D k-space and satisfies the necessary machine, time and space-filling constraints. The trajectory is defined as a continuous curve and, along this curve, measurements are made at uniform time intervals (e.g., one point every 4 μs) determined by the sampling bandwidth of the scanner. The trajectory needs to satisfy the following three constraints.

(i) *Machine constraints*

Let $g(t)$ represent the value of the gradient of the scanner at time t , and $s(t)$ the slew rate. They are related to the trajectory as its first and second derivative, respectively. Hence, they can be viewed as the trajectories velocity and acceleration, respectively, and they must satisfy the constraints

$$|g(t)| \leq G_0, \quad g(t) = \frac{1}{\gamma} \dot{k}(t), \quad (2.1)$$

$$|s(t)| \leq S_0, \quad s(t) = \frac{1}{\gamma} \ddot{k}(t), \quad (2.2)$$

where the parameter γ is the gyromagnetic ratio. The constraints G_0 and S_0 are the maximum gradient and slewrate, and these values are machine dependent. For a 3 T GE scanner (General Electric Medical Systems, Milwaukee, WI, USA) the value for the maximum slewrate is 15 *G/cm/ms*, while the value for the maximum gradient is 4 *G/cm*. Typically, most care needs to be placed in not exceeding the slewrate constraint as it is rare for any reasonable MRI trajectory to exceed its gradient bound without first exceeding the slewrate bound.

(ii) *Time constraint*

While measuring the raw k-space data, there is a finite amount of time the signal can be measured before the nuclei need to be re-excited. This leads to the constraint, $t \leq T_{max}$. In our experiment using a 3T GE scanner, T_{max} should be smaller than 60 *ms*.

(iii) *Space-filling constraint*

Finally, the trajectory needs to be space-filling, i.e., it needs to satisfy the Nyquist-criterion (Haacke, Brown, Thompson and Venkatesan (1999)). To better understand this criterion, think of k-space as a lattice where the distance between each point is determined by $2\pi/FOV$, where FOV stands for the field-of-view of the reconstructed image. In order to not violate the Nyquist criterion we need to visit, long enough to make a measurement, each point in the lattice contained within some cubic or spherical region around the center of k-space. The size of the subregion we are able to transverse in the required time window will ultimately determine the spatial resolution of our subsequent image reconstruction.

We have carefully studied different classes of possible trajectories. In this paper we present a 3D analogue to EPI sampling (Mansfield (1977)), called Echo-Volumar Imaging (EVI) (Mansfield, Howseman and Ordidge (1989), Mansfield, Coxon and Hykin (1995); and Harvey and Mansfield (1996)). Mansfield implemented an EVI trajectory that sampled $64 \times 64 \times 8$ points in k-space. Here we introduce an alternative version. Though our design can be altered to take any cylindrical shape, we illustrate the method using a cubic trajectory.

An echo-volumar imaging trajectory

Our goal is to design an EVI trajectory that zigzags through 3D k-space with the goal of hitting each coordinate point on a 3D Cartesian grid. In our implementation, such a trajectory will travel from one end of k-space to the other in a straight line and thereafter move to the next line, by traveling along a half circle. This procedure is repeated until all N^3 lattice points are visited. The value of N is determined by the amount of k-space it is possible to cover while still satisfying the necessary constraints. The final trajectory consists of a collection of straight lines and half circles. To ensure that each straight line consists of the same number of points, each line should begin at the same speed u , accelerate in the first half of the line and de-accelerate in the second half. The trajectory should then travel in a half circle with constant speed u before starting the process again on the next line. Since the appropriate spacing between adjacent lattice points in k-space is $\Delta_k = (2\pi)^{-1}FOV$, the actual length of each line is $2m\Delta_k$ where $m = N/2$.

The first question that arises is how large to make the radius of the half circles in order to maximize the amount of k-space that can be covered in the allocated time window. Ultimately the radius determines whether one should sample adjacent lines on the grid or instead perform interleaved sampling. To

answer this question, consider a trajectory $k(t)$ which pieces together ρm^2 sections such that each section is composed of a straight line of length $2m\Delta_k$ and a half circle with radius r . The value of ρ depends on the shape of the sampling region, e.g., $\rho = 4$ for a regular cube and $\rho = 3$ for a cylinder with a regular hexagon base. Suppose that the trajectory has a fixed slew rate, $|\ddot{k}(t)| = \ddot{k}_*$, and that it begins with speed u , accelerates in the first half of the line, de-accelerates in the second half, and then travels in the half circle with constant speed u . Since $r = u^2/\ddot{k}_*$, the amount of time the trajectory spends in the half-circle is

$$t_1 = \pi \frac{r}{u} = \pi \frac{u}{\ddot{k}_*}. \quad (2.3)$$

Furthermore, since the trajectory spends time $2t_2$ in the straight line, with

$$ut_2 + \ddot{k}_* \frac{t_2^2}{2} = m\Delta_k, \quad (2.4)$$

the total travel time for the trajectory is given by

$$\begin{aligned} T &= \rho m^2 (t_1 + 2t_2) \\ &= \rho m^2 \left(\frac{\pi u}{\ddot{k}_*} + \frac{2}{\ddot{k}_*} \left\{ -u + \left(u^2 + 2m\Delta_k \ddot{k}_* \right)^{\frac{1}{2}} \right\} \right). \end{aligned} \quad (2.5)$$

Since Eq. 2.5 is increasing in u , it is minimized by choosing the smallest possible value of r which is given by $\Delta_k/2$. Hence, it is optimal to sample adjacent lines as in the case of two-dimensional echo-planar schemes. Since $r = u^2/\ddot{k}_*$, this provides $u^2 = \Delta_k \ddot{k}_*/2$ and

$$T = \rho m^2 \{ (\pi - 2) + 2(4m + 1)^{\frac{1}{2}} \} \left(\frac{\Delta_k}{2\ddot{k}_*} \right)^{\frac{1}{2}}. \quad (2.6)$$

The best strategy is therefore to make a small turn if we accelerate in the line. An example of such a trajectory starts at the point $(0, 0, z_{min})$ and moves along the z-axis to the point $(0, 0, z_{max})$. Upon reaching this point the trajectory makes a half circular loop over to the point $(1, 0, z_{max})$ and then continues along the z-axis in the opposite direction until it reaches $(1, 0, z_{min})$. The trajectory continues in a similar manner until it has completed a square spiral in the xy-plane (Figure 2.1A and B). Using this approach it is possible to sample the central portion of 3D k-space with dimensions $14 \times 14 \times 14$ in the allocated time window. Further information about the practical implementation of the trajectory can be found in a companion paper focusing on the MRI aspects of this work (Lindquist, Zhang, Glover and Shepp (2008)).

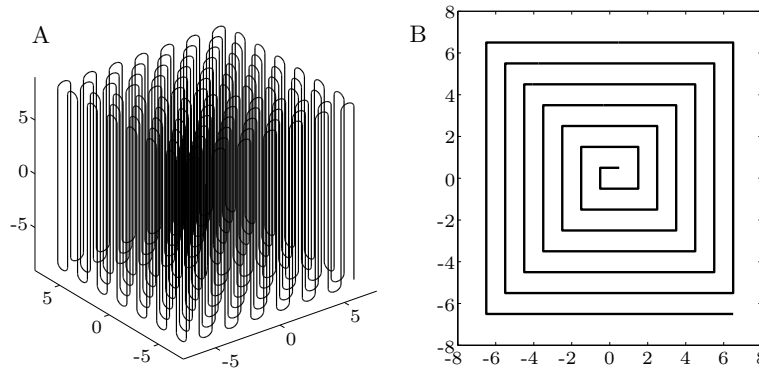


Figure 2.1. (A) An implementation of the echo-volumar imaging trajectory; (B) the echo-volumar imaging trajectory shown in (A) projected onto the xy -plane.

2.2. Reconstruction of EVI data

Once the central portion of 3D k -space has been collected, it needs to be transformed into image-space for statistical analysis. A standard approach toward reconstructing non-uniformly sampled k -space data is to interpolate the data onto a Cartesian grid (Jackson, Meyer, Nishimura and Macovski (1991)) and thereafter apply the fast Fourier transform (FFT). Our data is sampled on a Cartesian grid in the xy -plane, and it is relatively straightforward to use linear interpolation to get uniformly spaced measurements in the z -direction as well. After interpolation, our k -space data consists of 2,744 (e.g., $14 \times 14 \times 14$) uniformly sampled measurements in 3D k -space. As the data are sampled on a grid, reconstruction is straightforward using the FFT. The data are zero-filled to a resolution of $64 \times 64 \times 64$ prior to reconstruction, and a prolate spheroidal wave function filter (PSWF) (Shepp and Zhang (2000), Yang, Lindquist, Shepp, Zhang, Wang and Smith (2002), Lindquist (2003) and Lindquist, Zhang, Glover, Shepp and Yang (2006)) is applied to reduce truncation artifacts.

The PSWF is defined as the function, with support on a finite sub-region of k -space, whose inverse Fourier transform is maximally concentrated on a finite region of image-space, \mathbf{B} . Using the PSWF filter allows us to take the existing k -space data and reconstruct an image with a point spread function determined by the shape and size of the region \mathbf{B} . The amount of k -space sampled determines how small we can make the region \mathbf{B} and still obtain an efficient reconstruction with minimal Gibb artifacts. Ultimately, the diameter of \mathbf{B} has a reciprocal relationship with the amount of k -space that is sampled (Lindquist and Wager (2007)). Using this particular filter ties the reconstruction procedure together

with the spatial smoothing procedure. Ultimately, the spatial resolution using our approach is equivalent to that obtained after applying a Gaussian filter with FWHM of 12 *mm* to an image with dimensions $64 \times 64 \times 64$ and a FOV of 20 *cm*.

It should be noted that spatial smoothing is almost always performed prior to statistical analysis in fMRI using Gaussian filters with FWHM between 4–12 *mm* (Smith (2003)). Hence, while our method provides images on the low end of this spectrum, it is still on a comparable spatial resolution. However, it is important to remember that our images are obtained twenty times faster than the standard approach to acquiring 3D fMRI data. In the Discussion we discuss ways to further increase the spatial resolution of our data using multi-coil techniques. This is a major focus of future work.

2.3. Statistical analysis

After reconstruction, the statistical analysis of the image space data is conducted voxel-wise using a two-step procedure. In the first step we detect regions in the brain where there is a significant positive BOLD signal. These are the regions that would typically be categorized as having task-induced neuronal stimulation in a standard fMRI analysis. We are ultimately more concerned with detecting regions with significant negative BOLD signal. However, we feel it is a natural assumption that regions having a significant dip will also ultimately have a positive rise in BOLD signal if they are involved in the task at hand. This step therefore works as a simple screening process to remove uninteresting voxels, where there are no signs of task-induced activation, and allows for closer and more data-intensive inspection of voxels that are actually involved in the task. In the second step of the analysis we calculate the bootstrap distributions for the amplitude of the negative dip, as well as for the time when the negative dip reaches its peak (time-to-dip). Using these distributions we can perform statistical tests to determine whether there is a significant negative dip in a voxel, as well as compare the relative timing of the dips across various regions of the brain.

This second step is important as there is evidence that the negative dip is more localized to areas of neural activity (Yacoub, Shmuel, Pfeuffer, Van De Moortele, Adriany, Ugurbil and Hu (2001), Duong, Kim, Ugurbil and Kim (2000), Kim, Duong and Kim (2000) and Thompson, Peterson and Freeman (2004)) than the subsequent rise which appears less spatially specific. Hence, we may be able to prune away voxels that are simply adjacent to regions involved in the neuronal activity, rather than being directly involved. In addition, since the negative dip occurs in a time scale closer to that of the neural activity, there would appear to be fewer confounding factors influencing the order of the

time-to-dip in comparison to traditionally used metrics, such as the time-to-peak positive rise. Below is a more detailed outline of our two-step analysis.

Step One: After reconstructing the data into image-space we are left with a sequence of T three-dimensional images, each of size $64 \times 64 \times 64$. We model the fMRI time course using a classical decomposition model. The fMRI signal from voxel i , $i = 1, \dots, 64^3$ can be modeled as

$$Y_i(t) = \mu_i(t) + s_i(t) + z_i(t) + \epsilon_i(t). \quad (2.7)$$

Here $\mu_i(t)$ is a drift term which we model using a quadratic polynomial function

$$\mu_i(t) = \beta_0 + \beta_1 t + \beta_2 t^2. \quad (2.8)$$

The term $s_i(t)$ is a seasonal component that is due to heart rate and respiration. There are a number of possible ways to model this, but we use a finite impulse response (FIR) basis set which contains one free parameter for every time point of the response we seek to model. A FIR basis set is able to capture a response with arbitrary shape up to a given frequency limit determined by the periodicity of the seasonal component. Including this term adds d parameters to the model, where d is the periodicity of the seasonal component (in units of 0.1 s). We write this term as

$$s_i(t) = \sum_{j=1}^d \gamma_j(t) I_j(t) \quad (2.9)$$

where

$$I_j(t) = \begin{cases} 1 & \text{if } j = (t \bmod d) \\ 0 & \text{otherwise.} \end{cases} \quad (2.10)$$

The term $z_i(t)$ represents the BOLD response to the neuronal stimuli and it is the signal we are actually interested in studying. The shape of the BOLD response depends on the experimental condition, and can be modeled using a linear time-invariant system, where the stimulus function is the input and the hemodynamic response is the impulse response function, i.e.,

$$z_i(t) = \alpha \sum_{u=1}^{\infty} h(u) v(t-u). \quad (2.11)$$

Here α is an unknown scalar, $h(t)$ is the HRF and $v(t)$ is the known stimulus function which takes a value of 1 at time t if a stimulus is present, and 0 otherwise.

If the HRF is assumed to take a particular known shape, this model can be solved using the General Linear Model (GLM) framework (Worsley and Friston

(1995)), which is the standard approach toward fMRI data analysis. In this work, we use the canonical HRF (e.g., SPMs double gamma function). To increase its flexibility to handle slight temporal shifts in the onset of activation, we also include a term for the temporal derivative (Friston, Josephs, Rees and Turner (1998) and Henson et al. (2002)). This necessitates adding an additional parameter corresponding to the convolution of the stimulus function with the first derivative of the canonical HRF.

Finally, $\epsilon_i(t)$ is the noise present in the MR signal. Typically in fMRI, this is modeled either as an AR(p) or ARMA(1,1) process (Bullmore, Brammer, Williams, Rabe-Hesketh, Janot, David, Mellers, Howard and Sham (1996) and Purdon, Solo, Weissko and Brown (2001)). In this work we use an AR(2) process that adds three additional terms to our model. In summary our model can be formulated as

$$Y_i(t) = \sum_{j=0}^2 \beta_j t^j + \sum_{j=1}^d \gamma_j(t) I_j(t) + \alpha_1 \sum_{u=1}^{\infty} h(u) v(t-u) + \alpha_2 \sum_{u=1}^{\infty} \dot{h}(u) v(t-u) + \epsilon_i(t) \quad (2.12)$$

and has a total of $d+5$ regression parameters and 3 variance component parameters.

For each voxel, the model is fit using an iterative generalized least-squares approach, where the variance components and regression coefficients are alternatively calculated and updated. Thereafter, t-statistics corresponding to the HRF regressors are calculated, and statistical maps of the voxel-wise t-statistics are constructed. The maps are thresholded and corrected for multiple comparisons using the false detection rate (FDR) procedure (Benjamini and Hochberg (1995) and Genovese, Lazar and Nichols (2002)). This allows us to determine regions with statistically significant signal corresponding to the positive BOLD signal.

Step Two: The time courses from each of the voxels deemed active in Step One are extracted and analyzed further. They are decomposed into signal, trend and seasonality components (see Figure 2.2), and the seasonal and trend components are removed from the time course. The remaining time series is averaged over the m repetitions of the stimuli to obtain estimates of the HRF. Note that this approach is only feasible if the time between repetitions is as long, or longer, than the length of the HRF (e.g., 20 s). Using the estimated HRF from each voxel we can calculate the maximum amplitude of the positive rise, the minimum amplitude of the negative dip, as well as the time-to-peak for both the rise and dip.

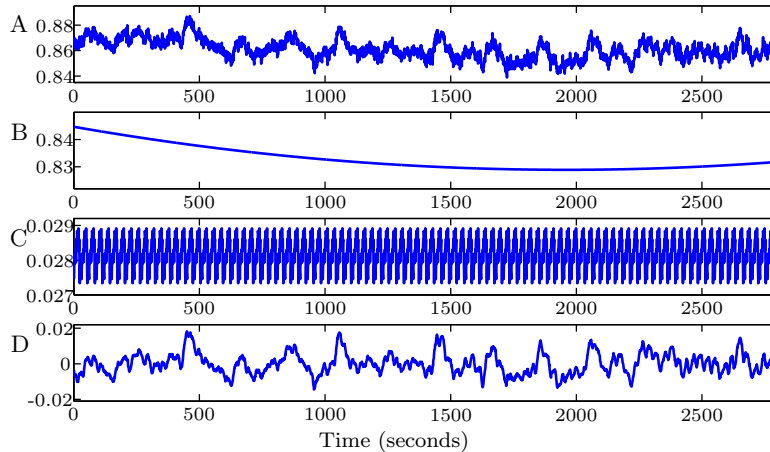


Figure 2.2. (A) A typical time course decomposed into (B) quadratic drift, (C) periodic nuisance parameters and (D) fMRI signal. The length of the period for the nuisance parameters is approximately 3 seconds and represents artifacts due to respiration.

Thereafter, for each time series, a statistical test based on the bootstrap method (Efron and Tibshirani (1998)) is performed to test whether the dips were statistically significant. Using resampling methods, a bootstrap distribution is calculated for both the peak amplitude of the negative BOLD response and the time-to-dip. This is done by taking a sample of size m with replacement from the m repetitions of the stimuli to create a new time course of the same length as the original. The time course is averaged over the m repetitions, and the amplitude and time-to-peak is recorded in a similar manner as for the original time series. This procedure is repeated 2,000 times to create a bootstrap distribution for the amplitude, as well as the time-to-dip. Using the bootstrap distribution for amplitude, tests are performed to determine whether the amplitudes of the dips are significantly different from zero.

Finally, for voxels with significant dips, a bootstrap distribution for the pairwise difference in time-to-dip is performed to determine whether the time-to-dip is significantly different between voxels across the brain. This allows us to determine the order in which the dip occurs in various regions associated with the task.

3. Experimental Design

Both the Cubic EVI trajectory and the reconstruction algorithm have been implemented in Matlab (Mathworks Inc.). To demonstrate the method's utility for dynamic studies, two high temporal resolution fMRI experiments were

designed to track the hemodynamic signals in the brain while the subject undergoes a visual-motor activation paradigm and an auditory-motor-visual activation paradigm.

The first activation paradigm consisted of fifteen cycles of 20 *s* intervals. At the beginning of each interval a 100 *ms* light flash was presented. The subject was instructed to press a button with their right thumb immediately after sensing the flash, thereby leading to activation of the motor cortex. During the 20 second interval, images were acquired rapidly every 100 *ms* using our cubic EVI trajectory. The sequence was repeated fifteen times, each time producing a dynamic data set of 200 temporal points.

The second activation paradigm also consisted of fifteen cycles of 20 *s* intervals. At the beginning of each interval a tone was sounded through headphones which the subject was wearing. The subject was instructed to press a button with their right thumb immediately after hearing the tone. Upon pressing the button a 100 *ms* light flash was presented, leading to activation of the visual cortex. During the 20 second interval, images were acquired rapidly every 100 *ms* using our cubic EVI trajectory. The sequence was repeated fifteen times, each time producing a dynamic data set of 200 temporal points. Reaction time data were collected that measured the time between the onset of the tone and the button press. As the flash appeared exactly 30 *ms* after the button press, the reaction time gives a measure of the timing of the appearance of the visual stimuli. This information was compared to the timing of the dip in the visual cortex for each cycle.

A healthy male volunteer participated in the study after giving informed consent in accordance with a protocol approved by the Stanford Institutional Review Board. In both experiments the first cycle was thrown out and the resulting data consisted of 14 cycles with a total of 2800 time units. The resulting k-space data was reconstructed and statistical analysis was performed as outlined in the previous section. The data were acquired with an effective TE 30 *ms*, flip angle 20 degrees, field of view $200 \times 200 \text{ mm}^2$, slice thickness 185 *mm* and bandwidth 125 *kHz*. The experiment was performed on a 3.0 *T* whole body scanner (GE magnet, General Electric Medical Systems, Milwaukee, WI, USA). T_2 -weighted FSE scans were obtained for anatomic reference (TR/TE/ETL = 3,000 *ms*/68 *ms*/12, 5 *mm* interleaved contiguous slices, FOV = 24 *cm*, 256×128 matrix).

4. Results

The feasibility of our rapid 3D imaging approach was tested experimentally using a visual-motor and an auditory-motor-visual stimulation paradigm, both described in the previous section. After data collection, the raw k-space data were

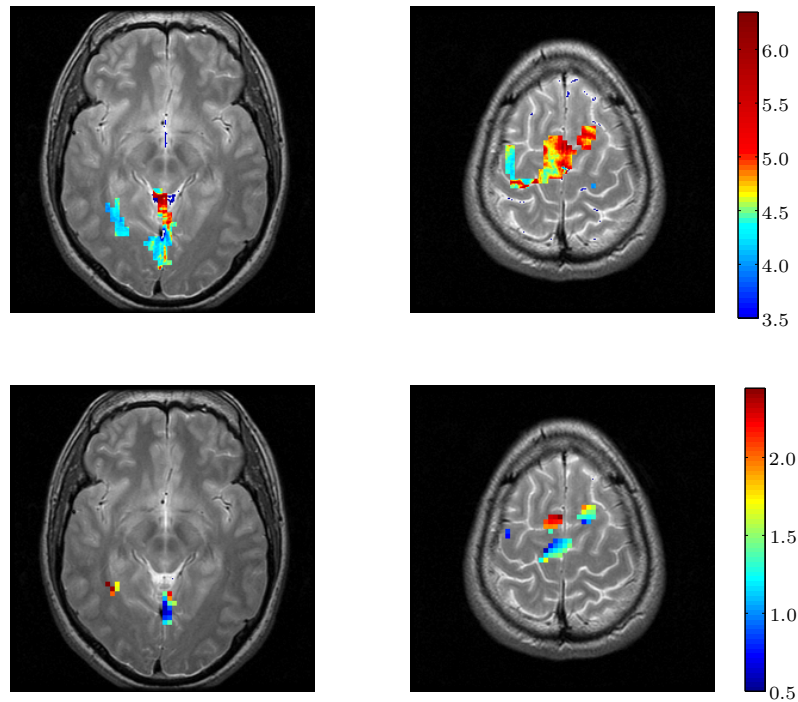


Figure 4.3. (Top row) Maps of the time-to-rise in voxels with significant activation for two slices in the visual-motor experiment. A slice containing the visual cortex is shown to the left and one showing the motor cortex to the right. The results indicate that the rise appears earlier in the visual than the motor cortex. (Bottom row) Maps of the time-to-dip in voxels with significant dips for the same two slices. The dip appears earlier in the visual than the motor cortex.

reconstructed into images of size $64 \times 64 \times 64$, and the time courses corresponding to the 64^3 voxels were analyzed for activation.

In a first step, statistical analysis was performed using the General Linear Model (GLM) approach. The design matrix consisted of three columns corresponding to a quadratic trend model for the signal drift, as well as d columns corresponding to the periodicity of the seasonal component. As the respiration was the dominant source of seasonality in the data we used its periodicity, which was empirically determined to be 3 seconds (i.e., $d = 30$), to determine the number of parameters. In addition, two extra parameters corresponding to the canonical HRF and its temporal derivative were added, giving a design matrix with 35 columns. The top row of Figure 4.3 shows examples of statistical parametric maps for two slices of the brain indicating voxels with significant task-

related activity (i.e., positive BOLD response) using a t-test ($p\text{-value} \leq 0.01$). A clear activation pattern is present both in the visual and motor cortices as would be expected. For voxels that were deemed active in the GLM analysis, their respective time courses were analyzed further. Each time course was decomposed into a trend component, a signal component and a seasonal component. Figure 2.2 shows the results of the decomposition of a representative time course. The quadratic trend and the seasonal component were removed from each time course and only the signal component is brought forth to the next stage of the analysis.

For each voxel deemed to have a significant rise according to the GLM analysis, the time-to-rise was estimated. Results for two slices, one centered in the visual and the other in the motor cortex, are shown in the top row of Figure 4.3. It is clear that the time-to-rise appears in the visual cortex prior to the motor cortex. Among active voxels, a statistical test based on the use of the bootstrap, was performed to test for significant dips ($p\text{-value} < 0.05$). The time-to-dip was estimated for active voxels and the results for the same two slices are shown in the bottom row of Figure 4.3. Again it is clear that the activation seems to be occurring in the visual cortex prior to that in the motor cortex.

Figure 4.4A shows the averages for two time courses extracted from the center of the visual and motor cortices, respectively. We clearly see that the HRF estimated from the visual cortex precedes the one estimated from the motor cortex throughout the course of the 20 second run. Figure 4.4B shows a close-up of the first 3 seconds following activation. A negative dip appears first in the visual cortex, as makes sense since the visual cortex is logically the first region of the brain that begins to work on the image. After a few hundred milliseconds delay we see a delayed negative response in the motor cortex. Bootstrap tests (Figure 4.4C–E) confirm these results, and show that while both dips are significant, the dip in the visual cortex occurs at a significantly earlier time point compared to that of the motor cortex. In this experiment both the timing of the dip and rise give compelling evidence that neuronal activity is taking place in the visual cortex prior to the motor cortex as would be expected by the experimental paradigm.

The same statistical analysis was repeated for the auditory-motor-visual stimulation paradigm. For each voxel deemed to have a significant rise according to the GLM analysis, the time-to-peak was estimated. Results for two slices, centered in the visual and motor cortices, respectively, are shown in the top row of Figure 4.5. It is important to note that in this experiment the order of activation should now be auditory, followed by motor, followed by visual. While the signal in the auditory does appear to peak first, there appears to be confounding in the timing of the peaks in the visual and motor cortices. This can be further seen in Figure 4.6 A, where clearly the signal over the motor cortex peaks *after*

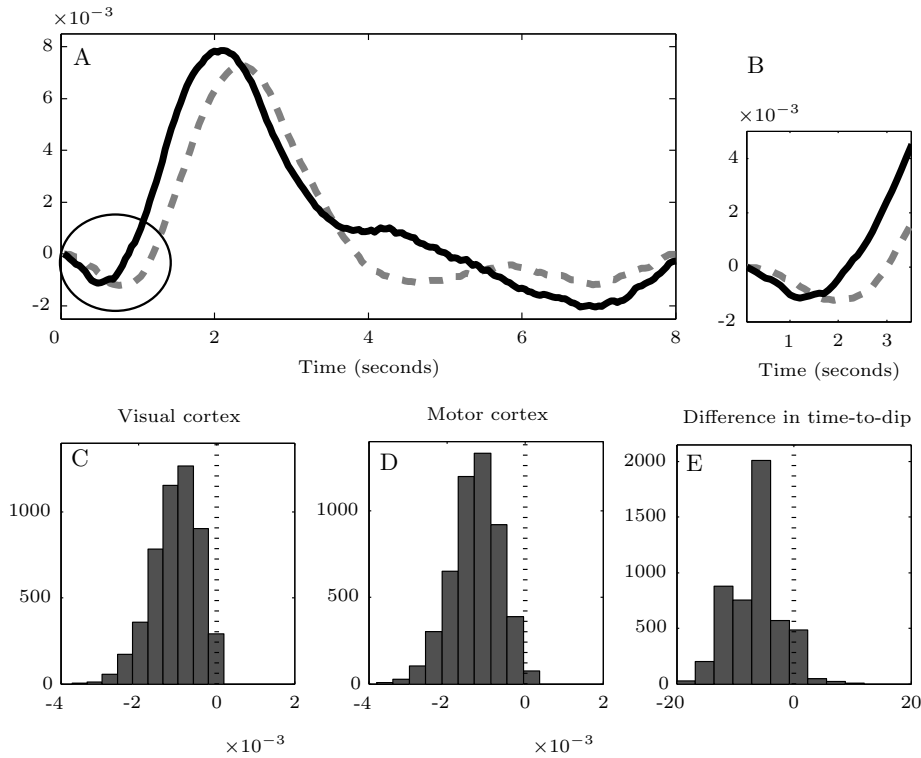


Figure 4.4. (A) Time courses from the visual (bold) and motor (dashed) cortices averaged over the 14 cycles of the visual-motor stimulus. (B) The first 3 seconds following stimulation for the two time courses appearing in (A). The dip appears earlier in the visual cortex than the motor cortex, which is consistent with the experimental paradigm. (C–E) The results of bootstrap tests show significant dips in both the visual and motor cortices, as well as a significant difference in time-to-dip between the two regions.

the visual cortex. However, studying the dip alleviates this confounding, as can be seen in both Figures 4.5 and 4.6B. The difference in the time-to-dip between the visual and motor cortices is not statistically different from zero. However, this is hardly surprising as the time between button press and visual stimuli is only 30 *ms*. A follow-up experiment should be performed to study how far apart these stimuli must lie in order for one to be able to discriminate between them. Included in Figure 4.6 is also the signal over the auditory cortex, whose dip and rise both peak prior to that of the visual and motor cortices. This is to be expected as the tone is presented before the button is pressed and the visual stimulus is presented.

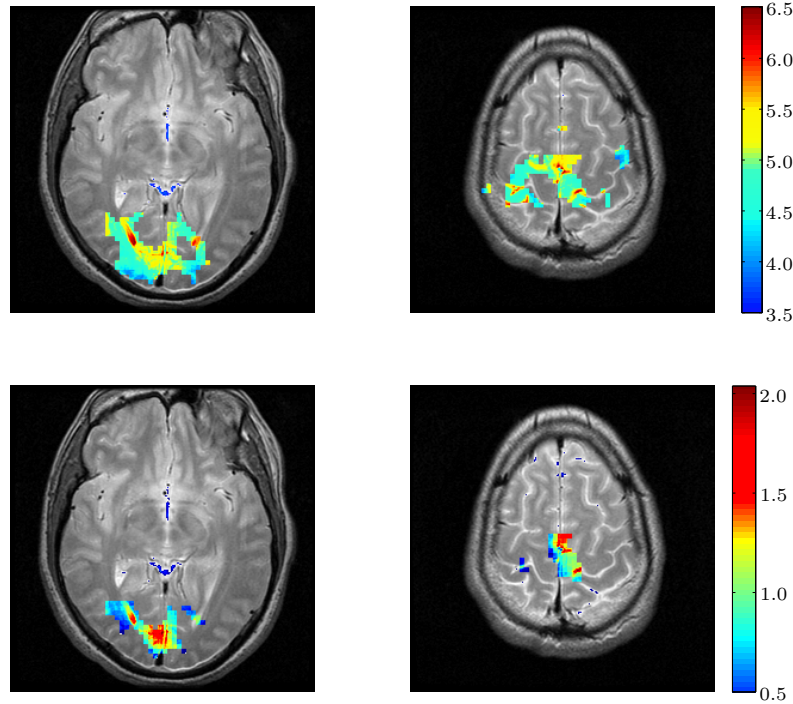


Figure 4.5. (Top row) Maps of the time-to-rise in voxels with significant activation for two slices in the auditory-motor-visual experiment. The slices that are included cover the visual (left) and motor cortices (right). (Bottom row) Maps of the time-to-dip in voxels with significant dips for the same two slices.

Finally, the time-to-dip in the visual cortex was manually read off for each individual cycle and compared to the corresponding reaction time data. The reaction time data gives a measure of the shift in the onset of the visual stimulus in each cycle. Cycles whose reaction times were outliers in the range of common reaction times were removed from the analysis, due to the influence they would have on the resulting correlation. Additionally, cycles without a clear dip were removed. Figure 4.7A shows a scatter plot of reaction time (in *ms*) against the time-to-dip (in *s*) for the 11 cycles that remained. The correlation between the two variables was 0.581. The relatively strong correlation indicates that the dip appears to be providing information about the onset of the underlying visual stimulus. A bootstrap distribution for the correlation was constructed by resampling with replacement 2,000 times from the 11 cycles. Using this distribution we were able to perform a significance test that indicated that the correlation was significantly larger than 0 (p -value= 0.0235). The bootstrap distribution is shown in Figure 4.7B.

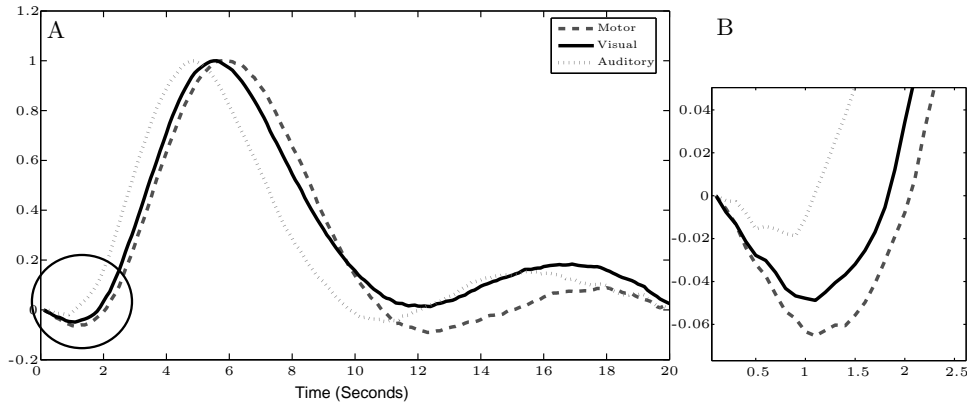


Figure 4.6. (A) Time courses from the auditory (dotted), visual (bold), and motor (dashed) cortices averaged over the 14 cycles. (B) The first 3 seconds following stimulation for the three time courses appearing in (A). The dip appears first in the auditory cortex, followed by the visual and motor cortices which are not statistically differentiable. The rise in the motor signal appears *after* the rise in the visual signal which implies an incorrect temporal ordering of activation.

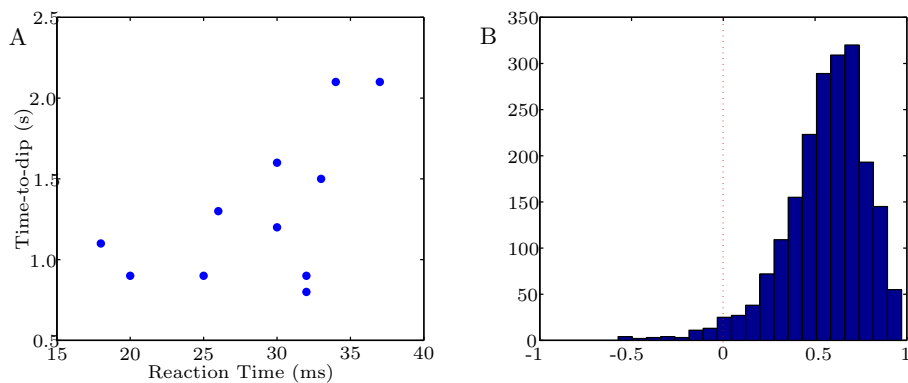


Figure 4.7 (A) A scatter plot of reaction times (in ms) against the time-to-dip (in s) for 11 cycles. The correlation between the two variables was determined to be 0.581. (B) A bootstrap distribution for the correlation was constructed by repeatedly resampling with replacement from the included cycles. Using the bootstrap distribution it was determined that the correlation was significantly larger than 0 ($p = 0.0235$).

To summarize the results of the experiments, we have shown reproducibly that significant dips are present in both the visual and motor cortices. In addition, there is a statistically significant difference in the time-to-dip between the

visual and motor cortices in our first experiment, which is consistent with the experimental paradigm. In the second experiment there is also a significant dip in the auditory cortex (again consistent with the paradigm) followed by dips in the visual and motor cortices which are not statistically differentiable. However, if we instead use the time-to-peak rise as a metric, the order of activation between the visual and motor cortices is confounded. This strengthens our notion that studying the initial negative BOLD response is a crucial tool for determining the timing of activation in the brain.

5. Discussion

This paper introduces a novel approach toward the acquisition and statistical analysis of rapid 3D fMRI data. There are a number of benefits to performing rapid imaging studies. First, it may allow one to study the initial negative BOLD response, instead of solely depending on the positive BOLD signal, for purposes of determining active regions as well as the order of activation in multiple active regions. Second, it allows for the efficient removal of physiological noise due to cardiac and respiratory effects. In a typical fMRI analysis, the time resolution is on the order of 2 seconds. Since respiration gives rise to a periodic function, with a period length of approximately 3 seconds, the Nyquist criteria does not allow us to fully reconstruct this signal. Rapid fMRI (with a temporal resolution on the order of 100 *ms*) circumvents this issue and allows for efficient reconstruction of the underlying signal without the problem of aliasing. This is beneficial as it allows us to significantly clean up the fMRI signal prior to analysis and to obtain more accurate estimates of the hemodynamic response function. Finally, rapid imaging alleviates issues related to the fact that spatially separate regions of the brain are sampled at different times, thus negating the need for slice-time correction. In addition, it may also allow for more accurate correction of subject motion, as movement occurring during the acquisition of each individual volume is reduced.

While the existence of the negative response remains controversial and has caused a great deal of debate, the idea of being able to systematically detect and perform inference about an early response to neuronal activity is appealing. While the results presented in this work are based on a single subject, they are done on different days and our statistical analyses confirm the negative dip based on all individual data sets. However, the experiments will ultimately need to be repeated on a larger group of subjects to gain more conclusive evidence of the existence of the initial negative response. The current work may therefore be seen as more of a proof of concept of our imaging and analysis procedure than a proof of our ability to reliably and reproducibly detect the initial negative BOLD signal in a population of subjects. Further experiments need to be performed to

determine (i) whether the dip can be reliably detected over multiple subjects, and (ii) whether in these subjects it provides an accurate picture of the timing of activation. However, we feel that if these results hold up, the technique would be an extremely valuable tool in neuroimaging studies.

In the data sets that are presented in this paper, we have shown reproducibly that significant dips are present in both the visual and motor cortices. In addition, there is a statistically significant difference in the time-to-dip between the visual and motor cortices in our first experiment, which is consistent with the experimental paradigm. In the second experiment there is also a significant dip in the auditory cortex (again consistent with the paradigm) followed by dips in the visual and motor cortices which are not statistically differentiable. However, if we instead use the time-to-peak rise as a metric, the order of activation between the visual and motor cortices is confounded. Our results indicate that the negative response may contain valuable information regarding the timing of activation, information that may be confounded when studying the positive BOLD response. This strengthens our notion that studying the initial negative BOLD response can be an important tool for determining the exact timing of activation in the brain.

It should be noted that in both experiments we performed there appears to be an increase in the number of false negatives when looking for voxels with significant dips compared to rise. This is made clear by comparing the two rows in Figures 4.3 and 4.5. The reason for this discrepancy may be due to the fact that the signal-to-noise ratio for the rise is on the order of 5 times larger than that of the dip. Alternatively, there is evidence that the initial negative BOLD response is more localized to areas of neural activity (Yacoub, Le and Hu (1998), Duong, Kim, Ugurbil and Kim (2000), Kim, Duong and Kim (2000) and Thompson, Peterson and Freeman (2004)) than the subsequent rise. Hence, the decreased number of active voxels may in fact be giving a more accurate picture of the true activation patterns in the brain. However, this statement is hard to verify, in part because the low spatial resolution provided by the current implementation of the method, and the fact that we have sacrificed spatial resolution to obtain our increase in temporal resolution proves to be somewhat of a liability in this respect. However, advances in multi-coil techniques (Sodickson and Manning (1997) and Pruessmann et al. (1999)) give an avenue to bridge this gap in the future. In these techniques, multiple k-space measurements can simultaneously be made and prior knowledge about RF field distributions or the image sensitivity of the coils can be utilized to construct images from under-sampled k-space data. We have recently implemented two new trajectories that allow us to obtain images with a temporal resolution of 100 *ms* and a spatial resolution on the order of $25 \times 25 \times 17$ and $46 \times 46 \times 17$, respectively. With the

latter spatial resolution we are quickly approaching the resolution that is used in standard fMRI experiments. However, the temporal resolution is increased 10-fold. These new trajectories constitute a second step in our rapid imaging method, and the results of these trajectories will be presented in future work.

6. Conclusions

A new approach toward rapid fMRI is introduced where a small central region of 3D k-space is sampled every 100 *ms* and a low spatial resolution snapshot of the brain with extremely high temporal resolution is obtained. In addition we introduce a new approach towards the statistical analysis of the resulting high-frequency fMRI data. The feasibility and efficiency of the combined acquisition and analysis approach is confirmed using data both from a visual-motor task and an auditory-motor-visual task. The increased temporal resolution allows us for the first time to perform a statistical analysis over the brain based solely on the initial negative BOLD response, rather than the sluggish positive BOLD response. In the visual-motor experiment there are coherent regions in both the visual and motor cortices with a significant initial negative BOLD signal. Further, the time to the peak negative response is shown to be significantly earlier in the visual cortex, consistent with the experimental paradigm. In the auditory-motor-visual experiment there is a significant dip in the auditory cortex followed by dips in the visual and motor cortices which are not statistically differentiable. However, if we instead use the time-to-peak positive BOLD response as a metric, the order of activation between the visual and motor cortices are confounded. This leads us to believe that studying the initial negative BOLD response can be an important tool for determining the timing of activation across different regions of the brain, though further experiments need to be performed to verify its reproducibility.

References

- Benjamini, Y. and Hochberg, Y. (1995). Controlling the false discovery rate: A practical and powerful approach to multiple testing. *J. Roy. Statist. Soc. Ser. B* **57**, 289-300.
- Bullmore, E. T., Brammer, M. J., Williams, S. C. R., Rabe-Hesketh, S., Janot, N., David, A. S., Mellers, J. D. C., Howard, R. and Sham, P. (1996). Statistical methods of estimation and inference for functional MR image analysis. *Magnetic Resonance in Medicine* **35**, 261-277.
- Buxton, R. and Frank, L. (1997). A model for the coupling between cerebral blood flow and oxygen metabolism during neural stimulation. *J. Cereb. Blood Flow Metab.* **17**, 64-72.
- Cho, Z. H., Ro, Y. M. and Lim, T. H. (1992). NMR venography using the susceptibility effect produced by deoxyhemoglobin. *Magnetic Resonance in Medicine* **28**, 25-38.
- Duong, T. Q., Kim, D. S., Ugurbil, K. and Kim, S. G. (2000). Spatio-temporal dynamics of the BOLD fMRI signals: Toward mapping columnar structures using the early negative response. *Magnetic Resonance in Medicine* **44**, 231-242.

- Efron, B. and Tibshirani, R. J. (1998). *An Introduction to the Bootstrap*. Chapman & Hall/CRC.
- Ernst, T. and Hennig, J. (1994). Observation of a fast response in functional MR. *Magnetic Resonance in Medicine* **32**, 146-149.
- Friston, K. J., Josephs, O., Rees, G. and Turner, R. (1998). Nonlinear event-related responses in fMRI. *Magnetic Resonance in Medicine* **39**, 41-52.
- Friston, K.J., Penny, W., Phillips, C., Kiebel, S., Hinton, G. and Ashburner, J. (2002). Classical and Bayesian Inference in Neuroimaging: Theory. *NeuroImage* **16**, 465-483.
- Gao, J. H., Xiong, J., Lai, S., Haacke, E. M., Woldorff, M. G., Li, J. and Fox, P. T. (1996). Improving the temporal resolution of functional MR imaging using keyhole techniques. *Magnetic Resonance in Medicine* **35**, 854-860.
- Genovese, C. R., Lazar, N. A. and Nichols, T. E. (2002). Thresholding of statistical maps in functional neuroimaging using the false discovery rate. *NeuroImage* **15**, 870-878.
- Haacke, E.M., Brown, R. W., Thompson, M. R. and Venkatesan, R. (1999). *Magnetic Resonance Imaging: Physical Principles and Sequence Design*. John Wiley, New York.
- Harvey, P.R. and Mansfield, P. (1996). Echo-volumar imaging (EVI) at 0.5 T: First whole-body volunteer studies. *Magnetic Resonance in Medicine* **35**, 80-88.
- Henson, R. N., Price, C. J., Rugg, M. D., Turner, R. and Friston, K. J. (2002). Detecting latency differences in event-related BOLD responses: application to words versus nonwords and initial versus repeated face presentations. *NeuroImage* **15**, 83-97.
- Irrazabal, P. and Nishimura, D. G. (1995). Fast three dimensional magnetic resonance imaging. *Magnetic Resonance in Medicine* **33**, 656-662.
- Jackson, J., Meyer, C. H., Nishimura, D. G. and Macovski, A. (1991). Selection of a convolution function for Fourier inversion using gridding. *IEEE Trans. Medical Imaging* **10**, 473-478.
- Kim, D. S., Duong, T. Q. and Kim, S. G. (2000). High-resolution mapping of iso-orientation columns by fMRI. *Nature Neuroscience* **3**, 164-169.
- Liang, Z. P. and Lauterbur, P. C. (1994). An efficient method for dynamic magnetic resonance imaging. *IEEE Trans. Medical Imaging* **13**, 677-686.
- Lindquist, M. A. (2003). Optimal data acquisition in fMRI using prolate spheroidal wave functions. *Internat. J. Imaging Systems and Technology* **13**, 803-812.
- Lindquist, M. A., Zhang, C. H., Glover, G., Shepp, L. A. and Yang, Q. X. (2006). A generalization of the two dimensional prolate spheroidal wave function method for non-rectilinear MRI data acquisition methods. *IEEE Trans. Image Process.* **15**, 2792-2804.
- Lindquist, M. A. and Wager, T. D. (2007). Spatial smoothing in fMRI using prolate spheroidal wave functions. To appear in *Human Brain Mapping* November, 2008.
- Lindquist, M. A., Zhang, C. H., Glover, G. and Shepp, L. A. (2008). Rapid three-dimensional functional magnetic resonance imaging of the initial negative BOLD response. *J. Magnetic Resonance* **191**, 100-111.
- Logothetis, N. (2000). Can current fMRI techniques reveal the micro-architecture of cortex? *Nature Neuroscience* **3**, 413.
- Malonek, D. and Grinvald, A. (1996). The imaging spectroscopy reveals the interaction between electrical activity and cortical microcirculation: implication for optical, PET and MR functional brain imaging. *Science* **272**, 551-554.
- Mansfield, P. (1977). Multi-planar image formation using NMR spin echoes. *J. Physics* **C10**, L55-L58.
- Mansfield, P., Howseman, A. M. and Ordidge, R. J. (1989). Volumar imaging using NMR spin echos: echo-volumar imaging (EVI) at 0.1 T. *J. Physics E* **22**, 324-330.

- Mansfield, P., Coxon, R. and Hykin, J. (1995). Echo-volumar imaging (EVI) at 3.0 T: First normal volunteer and functional imaging results. *J. Computer Assisted Tomography* **19**, 847-852.
- Menon, R. S., Ogawa, S., Hu, X., Strupp, J. S., Andersen, P. and Ugurbil, K. (1995). Bold based functional MRI at 4 Tesla includes a capillary bed contribution: echo-planar imaging mirrors previous optical imaging using intrinsic signals. *Magnetic Resonance in Medicine* **33**, 453-459.
- Mir, R., Guesalaga, A., Spiniak, J., Guarini, M. and Irarrazaval, P. (2004). Fast three-dimensional k-space trajectory design using missile guidance ideas. *Magnetic Resonance in Medicine* **52**, 329-36.
- Ogawa, S., Tank, D. W., Menon, R., Ellerman, J. M., Kim, S. G., Merkle, H. and Ugurbil, K. (1992). Intrinsic signal changes accompanying sensory stimulation: functional brain mapping and magnetic resonance imaging. *Proc. Nat. Acad. Sci.* **89**, 5951-5955.
- Ogawa, S., Lee, T. M. and Barrere, B. (1993). The sensitivity of magnetic resonance image signals of a rat brain to changes in the cerebralvenous blood oxygenation. *Magnetic Resonance in Medicine* **29**, 205-210.
- Ogawa, S., Menon, R., Tank, D. W., Kim, S. G., Merkle, H., Ellerman, J. M. and Ugurbil, K. (1993). Functional brain mapping by blood oxygenation level-dependent contrast magnetic resonance imaging: A comparison of signal characteristics with a biophysical model. *Biophysical J.* **64**, 803-812.
- Panych, L. P., Oesterle, C., Zientara, G. P. and Hennig, J. (1996). Implementation of a fast gradient-echo SVD encoding technique for dynamic imaging. *Magnetic Resonance in Medicine* **35**, 554-562.
- Pruessmann, K. P., Weiger, M., Scheidegger, M. B. and Boesiger, P. (1999). SENSE: sensitivity encoding for fast MRI. *Magnetic Resonance in Medicine* **42**, 952-956.
- Purdon, P. L., Solo, V., Weissko, R. M. and Brown, E. (2001). Locally regularized spatiotemporal modeling and model comparison for functional MRI. *NeuroImage* **14**, 912-923.
- Sabat, S., Mir, R., Guarini, M., Guesalaga, A. and Irarrazaval, P. (2003). Three dimensional k-space trajectory design using genetic algorithms. *Magnetic Resonance Imaging* **21**, 755-64.
- Shepp, L. A. and Zhang, C.-H. (2000). Fast functional magnetic resonance imaging via prolate wavelets. *Appl. Comput. Harmon. Anal.* **9**, 99-119.
- Smith, S.M. (2003). Preparing fMRI data for statistical analysis. In: *Functional MRI: An Introduction to Methods* (Edited by P. Jezzard, P. M. Matthews, S. M. Smith), Oxford University Press, Oxford, UK.
- Sodickson, D. K. and Manning, W. J. (1997). Simultaneous acquisition of spatial harmonics (SMASH): fast imaging with radiofrequency coil arrays. *Magnetic Resonance in Medicine* **38**, 591-603.
- Thompson, J. K., Peterson, M. R. and Freeman, R. D. (2004). High-resolution neurometabolic coupling revealed by focal activation of visual neurons. *Nature Neuroscience* **7**, 919-920.
- van Vaals, J. J., Brummer, M. E., Dixon, W. T., Tuithof, H. H., Engels, H., Nelson, R. C., Gerety, B. M., Chezmar, J. L. and den Boer, J. A. (1993). Keyhole method for accelerating imaging of contrast agent uptake. *J. Magn. Reson. Imaging* **3**, 671-675.
- Worsley, K. J. and Friston, K. J. (1995). Analysis of fMRI time-series revisited - again. *NeuroImage* **2**, 173-181.
- Yacoub, E., Le, T.H. and Hu, X. (1998). Detecting the early response at 1.5 Tesla. *NeuroImage* **7**, S266.

- Yacoub, E., Shmuel, A., Pfeuffer, J., Van De Moortele, P.F., Adriany, G., Ugurbil, K. and Hu, X. (2001). Investigation of the initial dip in fMRI at 7 Tesla. *NMR in Biomedicine* **14**, 408-412.
- Yang, Q. X., Lindquist, M. A., Shepp, L. A., Zhang, C. H., Wang, J. and Smith, M. (2002). The two dimensional prolate spheroidal wave function for MRI. *Journal of Magnetic Resonance* **58**, 43-51.
- Zientara, G. P., Panych, L. P. and Jolesz, F. A. (1994). Dynamically adaptive MRI with encoding by singular value decomposition. *Magnetic Resonance in Medicine* **32**, 268-274.

Department of Statistics, Columbia University, 1255 Amsterdam Ave., MC 4690 New York, NY 10027, U.S.A.

E-mail: martin@stat.columbia.edu

Department of Statistics, Rutgers University, 110 Frelinghuysen Rd., Piscataway, NJ 08854-8019, U.S.A.

E-mail: cunhui@stat.rutgers.edu

Department of Radiology, Stanford University School of Medicine, 300 Pasteur Drive Stanford, CA 94305-5105, U.S.A.

E-mail: gary@lucas.stanford.edu

Department of Statistics, Rutgers University, 110 Frelinghuysen Rd., Piscataway, NJ 08854-8019, U.S.A.

E-mail: shepp@stat.rutgers.edu

(Received April 2007; accepted January 2008)